

Lopsided and Bulging Distribution of Satellites around Paired Halos. II. 3D Analysis and Dependence on Projection and Selection Effects.

QINGLIN MA,¹ CHENG LI ¹ AND YANHAN GUO¹

¹*Department of Astronomy, Tsinghua University, Beijing 100084, China*

ABSTRACT

We investigate the distribution of subhalos in the vicinity of dark matter halo pairs in the Illustris-TNG simulation. The satellites around halo pairs with separations $d_{\text{sep}} > 0.5 h^{-1}\text{Mpc}$ exhibit a non-uniform distribution, which is a combined result of two distinct features: the “bulging” distribution, characterized by an overabundance along the pairwise direction, and the “lopsided” distribution, which shows an overabundance in the region between the paired halos. The bulging signal is stronger for halo pairs that are more widely separated and involve less massive halos, while the lopsidedness strengthens as the halo mass increases. Both signals depend weakly on halo mass ratio, and are primarily contributed by subhalos that are relatively distant from host halos. These measurements can be broadly reproduced by the overlap effect, provided the spatial alignment of halos is properly taken into account. Our results imply that the lopsidedness and bulging distribution may arise from two distinct origins: the former is caused simply by the overlap of two closely placed halos, while the latter is driven by the alignment of halos with large-scale filamentary structures. We examine the impact of projection and selection effects by conducting the same analysis of satellite distribution in two dimensions and in a mock catalog that replicates the selection effects of the SDSS galaxy sample. We find that the 3D-to-2D projection significantly suppresses the bulging distribution, with particularly strong effects at large pair separations, low halo masses, and large halo mass ratios.

Keywords: methods: numerical - cosmology: theory - dark matter - galaxies: formation - galaxies: haloes - large-scale structure of universe

1. INTRODUCTION

Matter distribution in the universe is not uniform on scales smaller than a few hundred Mpc. Instead, it presents a complex pattern known as the cosmic web (Bond & Myers 1996), comprising interconnected *filaments* of galaxies and gas, dense galaxy clusters and massive dark matter halos (*nodes*), vast empty regions (*voids*), and flattened *walls*. The cosmic web serves as a manifestation of the intricate large-scale structure (LSS) of the universe, shaped by gravitational collapse due to dark matter and negative pressure due to dark energy, in addition to cosmic expansion. Therefore, understanding the cosmic web is crucial for shedding light on galaxy for-

mation, dark matter properties, and cosmological models.

In particular, the cosmic web is believed to play vital roles in regulating the orientations of both dark matter halos and galaxies, as well as the anisotropic distribution of their surrounding subhalos and satellite galaxies. For instance, the tidal field generated by the cosmic web is capable of distorting the collapsing protogalactic halos (Peebles 1969; Doroshkevich 1970; White 1984), contributing to the anisotropic accretion of satellites (Knebe et al. 2004; Aubert et al. 2004; Libeskind et al. 2005; Zentner et al. 2005; Wang et al. 2014; Shao et al. 2018), and subsequently shaping the alignment between halo and galaxy orientations and the large-scale filamentary structure (Faltenbacher et al. 2009; Zhang et al. 2009; Paz et al. 2011; Libeskind et al. 2012; Schneider et al. 2012; Li et al. 2013; Forero-Romero et al. 2014; Libeskind et al. 2015; Kang & Wang 2015; Ganeshiah Veena et al. 2018).

Corresponding author: Qinglin Ma
maq121@mails.tsinghua.edu.cn

Corresponding author: Cheng Li
cli2015@tsinghua.edu.cn

The anisotropic distribution of satellites has been observed around both isolated galaxies in our universe and dark matter halos in numerical simulations. This anisotropy manifests as two distinct features: a lopsided distribution with an overabundance of satellites located on one side of their host halos or central galaxies (Brainerd & Samuels 2020; Wang et al. 2021; Samuels & Brainerd 2023; Heesters et al. 2024), and a bulging distribution, characterized by the preferential location of satellites along the major axis of the host halos or central galaxies (Faltenbacher et al. 2008; Libeskind et al. 2014; Tempel et al. 2015; Gu et al. 2022). It is well established that both the bulging and lopsided satellite distributions around isolated halos or galaxies originate from the large-scale tidal field and the anisotropic accretion of galaxies and subhalos (e.g., Knebe et al. 2004; Aubert et al. 2004; Libeskind et al. 2005; Zentner et al. 2005; Kang & Wang 2015; Liu et al. 2024).

The anisotropic distribution of satellites has also been observed around pairs of galaxies or dark matter halos. For instance, a lopsided distribution has been reported for the satellite galaxies in the Local Group, which are preferentially located in the region between the Milky Way (MW) and M31 (McConnachie & Irwin 2006; Conn et al. 2013; Ibata et al. 2013). Furthermore, Libeskind et al. (2016) examined the satellites around a sample of galaxy pairs similar to the MW-M31 system, statistically detecting a similarly anisotropic distribution. This anisotropy is characterized not only by a lopsided feature with elongated filamentary structures, but also by a bulging feature, where more satellites are observed along the line connecting the galaxy pairs than those seen perpendicular to it. In line with this, Pawlowski et al. (2017) conducted a search for analogous anisotropy in the Local Group analogs within cosmological simulations.

In a parallel paper (Guo, Ma & Li, submitted to APJ; hereafter Paper I), we have extended the study of lopsided and bulging distributions of satellites around halo pairs, by selecting a sample of paired central galaxies from the Sloan Digital Sky Survey (SDSS; York et al. 2000) and examining the lopsidedness and bulging signals as function of host halo mass, halo mass ratio and pair separation. In addition, we have constructed a mock catalog that has the same selection effects as the observational sample, based on the Illustris-TNG300 simulation. By incorporating the orientation of individual galaxies and the alignment of galaxy/haos orientation with halo pair orientation, our mock catalog successfully reproduces the lopsided and bulging distributions of satellites across halo pairs of various properties. Our results demonstrate that the angular distribu-

tion of satellites is a natural phenomenon of the Λ CDM model, eliminating the need to introduce other mechanisms such as the local gravitational effects proposed by Libeskind et al. (2016).

In this work, we perform a three-dimensional (3D) analysis of the lopsided and bulging distribution of satellites around pairs of dark halos, examining the potential biases in the observational measurements caused by projection and selection effects in redshift surveys. For this purpose, we measure the angular distribution of subhalos in and around halo pairs with varying separations, halo masses, and halo mass ratios, similar to our approach in Paper I. In particular, we obtain measurements in three-dimensional space using the full simulation box, in addition to those in a projected two-dimensional plane and in redshift space using a mock catalog that mimics the selection effects of SDSS-like surveys. By comparing the results from these three different conditions, we aim to discern the influence of projection and selection effects on the angular distribution of satellites, as observed in previous studies. As we will demonstrate, the projection effect significantly weakens the bulging distribution of satellites in halo pairs but has a negligible effect on their lopsided distribution. The three-dimensional analysis confirms that the scenario revealed by Paper I and previous studies based on observational samples remains broadly valid.

In what follows, we first present 3D analyses of the satellite distribution around halo pairs and overlapping halos in section 2. We then investigate the influence of projection and selection effects in section 3. We discuss in section 4 and conclude in section 5.

2. 3D ANALYSIS

2.1. *Satellite distribution around halo pairs*

Throughout this work, we make use of the *Next Generation Illustris* dark matter only simulation (IllustrisTNG-ODM; Marinacci et al. 2018; Naiman et al. 2018; Nelson et al. 2018; Springel et al. 2018; Pillepich et al. 2018), which contains 2500^3 dark matter particles, each with a mass of $7 \times 10^7 h^{-1} M_\odot$, in a periodic box of size $L = 205 h^{-1} \text{Mpc}$ on a side. The adopted cosmology parameters are: $\Omega_m = 0.3089$, $\Omega_b = 0.0486$, $\Omega_\Lambda = 0.6911$, $h = 0.6774$, $\sigma_8 = 0.8159$, and $n_s = 0.9667$. Dark matter halos and subhalos are identified using the friends-of-friends (FoF; Davis et al. 1985) and the `subfind` (Springel et al. 2001) algorithms, respectively. Throughout this work, we focus our analysis on the local universe, thus using only the simulation snapshot at $z = 0$.

From the simulation, we select halo pairs in three dimensions, requiring that the involved halos in each pair are separated by a distance in the range of $0 <$

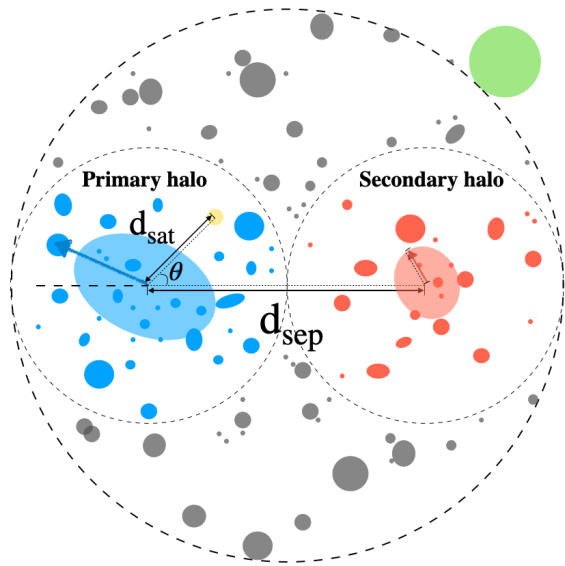


Figure 1. The schematic of a typical halo pair is illustrated, where the more massive halo (primary, depicted in blue) and the less massive halo (secondary, depicted in red) are separated by a distance of d_{sep} . Subhalos located within a radius of $0.5d_{\text{sep}}$ from the two halos are considered “satellites”, represented by red and blue ellipsals enclosed by thin dashed circles. For a given satellite at a distance of d_{sat} from its host halo, the position angle θ is defined as the angle between the line connecting the satellite to its halo and the line connecting the paired halos. The large dashed circle, which is centered at the midpoint of the pair connection line and has a radius of d_{sep} , represents the exclusion boundary, within which there must be no third halo that is more massive than half of the primary halo mass. See the text for further details.

$d_{\text{sep}} < 2h^{-1}\text{Mpc}$ and have masses in the range of $10^{11.6}h^{-1}M_{\odot} < M < 10^{15.6}h^{-1}M_{\odot}$. The halo mass is defined as the total dark matter mass within the virial radius R_{vir} , within which the average matter density is 102 times the critical density of the universe. Additionally, there must be no third halo within a radius equal to the pair separation d_{sep} from the midpoint of the line connecting the two halos. For a given pair, the more massive halo is referred to as the *primary halo*, while the less massive one is referred to as the *secondary halo*. These restrictions give rise to a sample of 25,139 halo pairs at $z = 0$. We note that our selection criteria are similar to those adopted in Gong et al. (2019), but we have adopted wider ranges for pair separation and halo mass. This allows us to extend the analysis to more general cases beyond those resembling the Local Group.

Figure 1 presents a schematic diagram of the halo pairs. Following Gong et al. (2019), we consider all the subhalos located within $d_{\text{sep}}/2$ from the nearer halo when measuring the satellite distribution for a halo pair.

This includes not only the subhalos within the virial radii of the two halos but also some of those located outside (as indicated by the blue and red colors in the figure). For each subhalo in consideration, we measure its positional angle θ , defined as the angle between its position vector with respect to the nearer halo and the line connecting the two halos. Defined this way, angles in the range of $0 \leq \theta \leq 90^\circ$ (or equivalently $0 \leq \cos \theta \leq 1$) correspond to subhalos located in the internal region between the two halos, while angles in the range of $90^\circ < \theta \leq 180^\circ$ (or equivalently $-1 \leq \cos \theta < 0$) correspond to those located on the outer sides.

Figure 2 displays the distribution of $\cos \theta$ for halo pairs with varying primary halo masses (M_p), pair separations (d_{sep}), and secondary-to-primary halo mass ratios (M_s/M_p). Additionally, Figure 3 compares the $\cos \theta$ distribution for subhalos at different distances from their host halo, as measured for halo pairs in different primary halo mass bins. Overall, $\cos \theta$ presents a non-uniform distribution for halo pairs with separations $d_{\text{sep}} > 0.5 h^{-1}\text{Mpc}$, showing a minimum of $P(\cos \theta)$ around $\cos \theta = 0$ and increased values towards both $\cos \theta = 1$ and $\cos \theta = -1$. This indicates a “bulging” distribution of satellites around the halo pairs, characterized by an overabundance of satellites along the connection line of the halo pairs, both inside and outside the pairs. The bulging signal is stronger for halo pairs that are more widely separated and involve less massive halos, but it exhibits a rather weak dependence on the secondary-to-primary halo mass ratio. As shown by Figure 3, the bulging signal at a given halo mass is primarily contributed by subhalos located relatively distant from their host halos.

In addition, lopsidedness is also observed for halo pairs with $d_{\text{sep}} > 0.5 h^{-1}\text{Mpc}$, indicating that satellites tend to be preferentially located inside the halo pairs ($\cos \theta > 0$) rather than outside ($\cos \theta < 0$). This signal strengthens as the halo mass increases, but it shows weak dependence on the pair separation. Similar to the bulging distribution, the lopsided distribution also exhibits a weak dependence on the halo mass ratio and is primarily attributed to more distant subhalos.

In contrast, the subhalos around close halo pairs with $d_{\text{sep}} < 0.5 h^{-1}\text{Mpc}$ appear to exhibit relatively uniform distributions, or even slightly higher abundances on the outer sides, though this is associated with large uncertainties. It is important to note that these close pairs are dominated by relatively low-mass halos and consist of halos with comparable masses. As a result, they are likely merging systems and dynamically unstable, leading to different processes regulating the satellite distri-

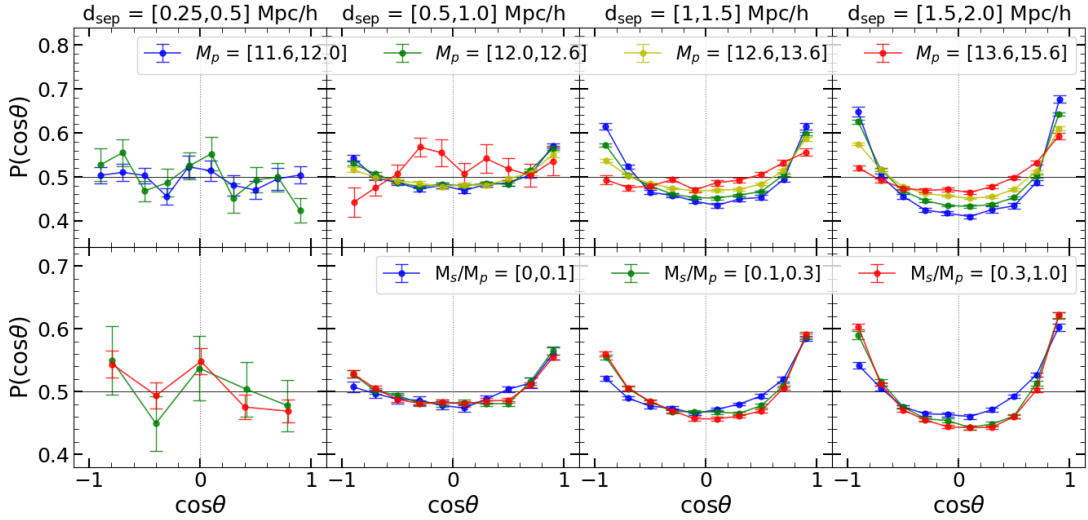


Figure 2. Satellite distribution in 3D as measured by $P(\cos\theta)$ is shown for halo pairs of varying separation d_{sep} , primary halo mass M_p , and secondary-to-primary halo mass ratio M_s/M_p , as indicated. The horizontal line indicates the uniform distribution.

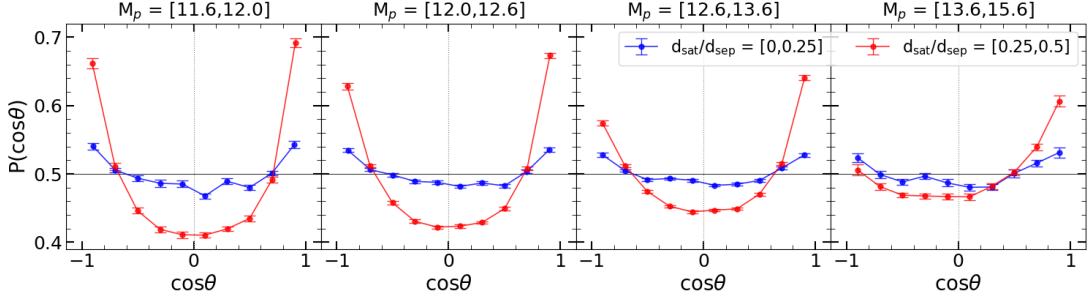


Figure 3. Satellite distribution $P(\cos\theta)$ is shown for halo pairs of different primary halo masses, as well as different satellite-to-host distance for given halo mass, as indicated.

bution around these pairs compared to the other halo pairs in our sample.

2.2. Satellite distribution around overlapping halos

One possible explanation for the lopsided and bulging distribution of satellites around paired halos is the so-called ‘‘overlap effect’’: an overabundance of satellites is naturally found between two halos when they are brought closer together, along with their surrounding satellite distribution. In previous studies, this hypothesis has been tested by comparing the satellite distribution around actual halo pairs with that around overlapping halos. For each actual halo pair, two halos with masses similar to those of the halos in the pair are selected from the simulation, and along with their surroundings, they are placed at the same separation as the actual halo to form the corresponding overlapping halos. In practice, we require the overlapping halos to be closely matched in mass with the corresponding halos in the actual pairs, with a tolerance of $\Delta \log_{10} M_h \leq 0.1$, and to be separated at the same distance as the ac-

tual halo pair, with a tolerance of $\Delta d_{\text{sep}} \leq 0.5 h^{-1} \text{Mpc}$. For each of the actual pairs, this process is repeated 20 times, resulting in a sample of overlapping halos that is 20 times the size of the actual pair sample.

Measurements of the satellite distribution around the overlapping halos at different separations are plotted as green shaded regions, categorized by different primary halo masses in Figure 4, by various halo mass ratios in Figure 5, and by different satellite-to-host distances in Figure 6. The corresponding measurements for the actual halos obtained earlier are plotted as black circles with error bars for comparison. Generally, the overlapping halos present no bulging signals but show only a lopsided distribution, with satellites being preferentially found between the two halos. Overall, the lopsidedness is relatively weak and matches that of the actual halo pairs only for close pairs with $d_{\text{sep}} < 0.5 h^{-1} \text{Mpc}$ or for those involving the most massive halos ($M_p > 10^{13.6} h^{-1} M_\odot$), where the signals in actual halo pairs are also weak. This result indicates that the overlap effect alone is insufficient, and additional mechanisms are

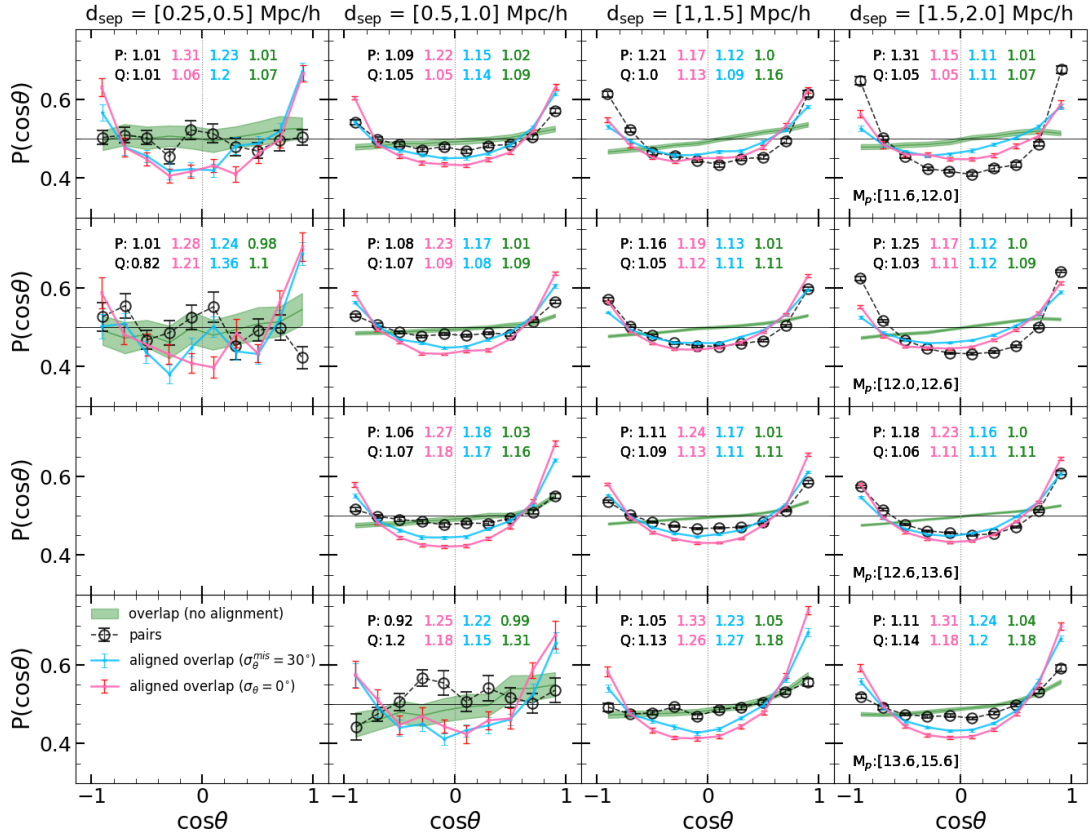


Figure 4. Satellite distribution $P(\cos\theta)$ for halo pairs of different pair separations (panels from left to right) and primary halo masses (panels from top to bottom), as indicated. In each panel, different symbols/lines/colors represent the results of different samples, including the actual halo pairs (black circles), the overlap sample without alignment (green), and the aligned overlap samples with a misalignment angle of zero (magenta) or 30° (cyan). The P and Q parameters quantifying the bulging and the lopsidedness in the satellite distribution are indicated in each panel, with the colors corresponding to the different samples.

required to fully explain the satellite distribution around halo pairs.

When constructing the overlap sample, the two overlapping halos are randomly oriented, as done in previous studies. However, as pointed out in Paper I, dark matter halos are not oriented at random; rather, they are preferentially aligned with large-scale filamentary structures, a fact that has been well established both for dark halos in simulations and for galaxies and groups of galaxies in redshift surveys. Following Paper I, we incorporate the alignment of halos in the overlap sample, by aligning the orientation of the two overlapping halos with their connection line, which is known to be somewhat aligned with large-scale filaments (e.g. Tempel & Tamm 2015; Mesa et al. 2018; Lamman et al. 2024; Rong et al. 2024; Sarkar & Pandey 2024). To determine the orientation of halos, we use the dark matter particles within R_{vir} to calculate the weighted inertia tensor for each halo (Allgood et al. 2006). Assuming the halo can be modeled by a triaxial ellipsoid, we then determine the three axes of the halo by the eigenvectors of the inertia tensor, with

the major axis given by the eigenvector corresponding to the largest eigenvalue. For each pair of overlapping halos in the overlap sample, we rotate the entire configuration of subhalo distribution around each of the two halos, ensuring that the major axes of the two halos are aligned with each other.

The measurements of $P(\cos\theta)$ for the “aligned overlap sample” constructed in this manner are additionally plotted as magenta lines in Figure 4, Figure 5, and Figure 6. Furthermore, we randomly rotate the major axis of the overlapping halos to mimic the misalignment of halo orientations found in previous studies (e.g. Faltenbacher et al. 2009; Okumura et al. 2009). We adopt a Gaussian distribution for the misalignment angle, with a mean of zero and a width of $\sigma_{\text{mis}} = 30^\circ$. Here, σ_{mis} is chosen to represent the average misalignment of different types of galaxies, which have been found to be $25^\circ - 35^\circ$ for red galaxies and $25^\circ - 65^\circ$ for blue galaxies (Wang et al. 2008; Okumura et al. 2009). The measurements of $P(\cos\theta)$ for this “misaligned overlap sample” are plotted as cyan lines in the same figures.

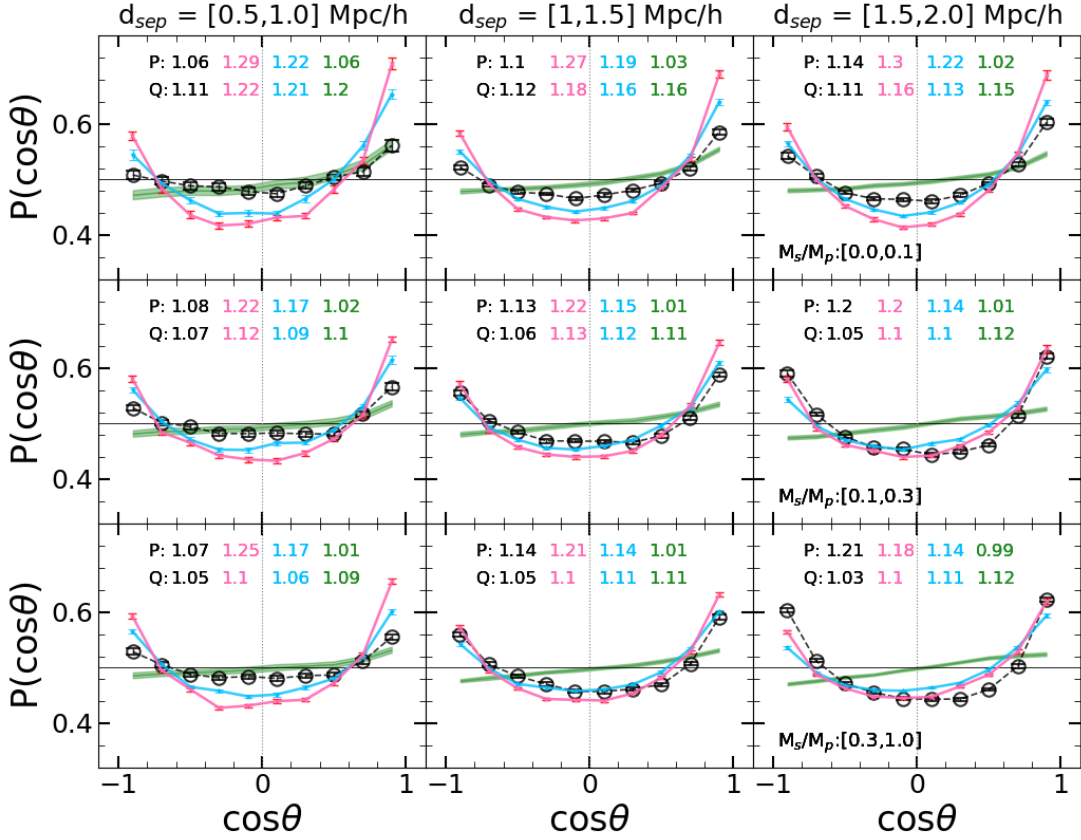


Figure 5. Satellite distribution $P(\cos\theta)$ for halo pairs of different pair separations and secondary-to-primary halo mass ratios, as indicated. The symbols and colors are the same as in Figure 4.

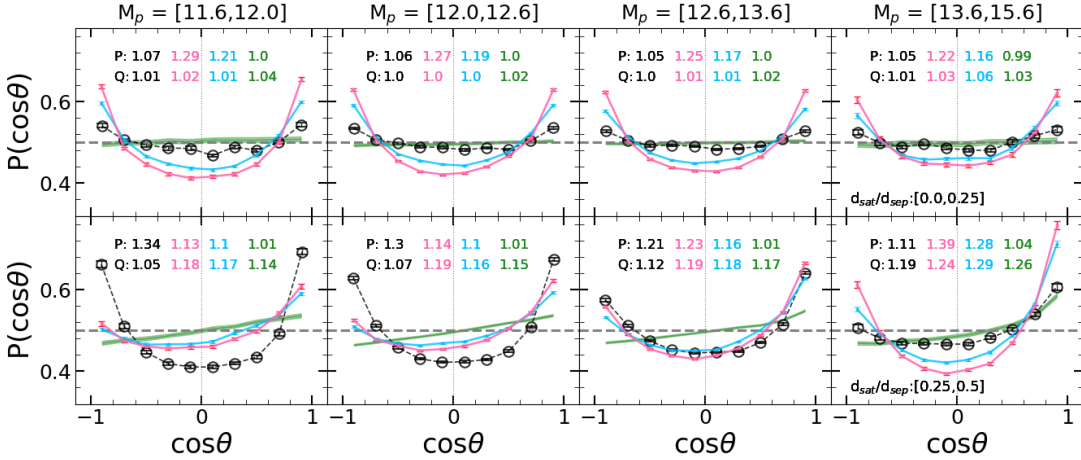


Figure 6. Satellite distribution $P(\cos\theta)$ for halo pairs of different primary halo masses and satellite-to-host distances, as indicated. The symbols and colors are the same as in Figure 4.

To enable quantitative comparisons, we define two parameters, P and Q , to respectively quantify the strength of the bulging and lopsidedness signals. Specifically, P is defined as the integral of $P(\cos\theta)$ over the ranges $0.5 < \cos\theta < 1.0$ and $-1.0 < \cos\theta < -0.5$, divided by the integral of $P(\cos\theta)$ over the range $-0.5 <$

$\cos\theta < 0.5$. This parameter measures the relative abundance of satellites along the direction of the pair orientation compared to that perpendicular to it. Following Gong et al. (2019), the Q parameter is defined as the ratio of $P(\cos\theta)$ at $0.8 < \cos\theta < 1.0$ to that at $-1.0 < \cos\theta < -0.8$, thereby measuring the relative

satellite abundance between the inner and outer sides of the halo pair. The P and Q parameters are calculated for all the $P(\cos\theta)$ measurements, as indicated in each panel of Figure 4, Figure 5, and Figure 6.

As can be seen from the figures and according to the P and Q parameters, after the alignment of halos is included, the satellite distribution in all cases becomes strongly bulging, while the lopsidedness remains similar. The inclusion of misalignment only slightly weakens the bulging signal. Consequently, both the “aligned” and “misaligned” overlap samples can roughly replicate the behaviors of actual halo pairs in most cases, but they overpredict the bulging signal for close pairs or pairs with massive halos, where the original, randomly placed overlapping halos provide better agreement. This result implies that the lopsidedness signal and the bulging signal may arise from two distinct origins: the bulging relates to the alignment of halo orientation and subhalo distribution with large-scale filamentary structures, which is significant for relatively widely separated pairs of less massive halos, and the lopsidedness is simply the overlap effect, which applies to pairs of all cases but plays a dominant role only for pairs of massive halos or substantially close pairs of low-mass halos. We will revisit this topic and discuss it further in subsection 4.2.

3. PROJECTION AND SELECTION EFFECTS

Observational studies of galaxy distribution rely on imaging and flux-limited samples, which suffer from projection and complex selection effects. It is crucial to consider these effects before properly interpreting the observational results. In this section, we examine the satellite distribution around halo pairs and overlapping halos, both in two dimensions by projecting the simulation box onto a 2D plane, and in redshift space by constructing mock catalogs that replicate the selection effects of real galaxy surveys.

3.1. Satellite distribution around halo pairs

For the 2D analysis, we take the $x - y$ plane of the IllustrisTNG-ODM simulation as the projection plane. We have verified that our results remain unchanged when using the $x - z$ or $y - z$ planes. We select halo pairs on the 2D plane, requiring them to have halo masses in the same range as those analyzed in 3D. Additionally, these pairs must have projected separations in the range of $0 < d_{\text{sep}}^{\text{proj}} < 2 h^{-1}\text{Mpc}$ and velocity differences $d_v < 1000 \text{ km/s}$ along the line of sight (LoS), specifically the z -axis. We account for both the position difference and the peculiar velocity difference when calculating the velocity difference d_v between two given halos. Similar to the halo pairs selected in 3D, each of the projected

halo pairs is additionally required to have no third halo within a cylinder centered at the midpoint of the halo pair, which has a projected radius equal to $d_{\text{sep}}^{\text{proj}}$ and a LoS depth of $\pm 1000 \text{ km/s}$. All subhalos located within $0.5d_{\text{sep}}^{\text{proj}}$ in projection and $\pm 500 \text{ km/s}$ along LoS from the nearer halo are considered satellites around the halo pair. For each satellite, we calculate the angle in the projection plane, Θ , defined as the angle between the line connecting the satellite to the nearer host halo and the line connecting the two halos. Similar to the case in 3D, a satellite is labeled as being located “inside” the halo pair if $\Theta \in (0^\circ, 90^\circ)$ and as being “outside” if $\Theta \in (90.0^\circ, 180.0^\circ)$.

For the analysis of observational selection effects, we have constructed a mock catalog using the approach described in detail in Paper I. In short, assuming each subhalo in the simulation hosts a galaxy, we assign a stellar mass M_* and an r -band absolute magnitude M_r to each galaxy by applying the subhalo abundance matching model and the M_* versus M_r relation derived from the SDSS. We then use the model galaxies to construct the mock catalog, which incorporates the same selection effects as the SDSS galaxy sample, including redshift-dependent incompleteness due to the limiting magnitude and sky position-dependent incompleteness across the survey footprint, among other effects. From the mock catalog, we identify pairs of central galaxies as proxies for halo pairs and measure the angular distribution of satellite galaxies around each halo pair in the same way as described above in our 2D analysis. As shown in Paper I, the mock catalog successfully reproduces the observational measurements of $P(\Theta)$ for halo pairs of varying pair separations, primary halo masses, and secondary-to-primary halo mass ratios, as obtained from the SDSS galaxy sample.

In Figure 7 and Figure 8, we compare the satellite distribution around halo pairs as measured by $P(\Theta)$ on the projection plane (red lines) and in the mock catalog (blue symbols), for halo pairs with different separations, halo masses, and halo mass ratios. Note that the two lowest mass bins from previous figures have been combined into a single mass bin, $11.6 < \log_{10}(M_p[M_\odot/h]) < 12.6$, in order to avoid the relatively large Poisson noise present in those narrow bins in the mock catalog. As can be seen, the satellites selected in 2D and those from the mock catalog display very similar distributions around halo pairs with relatively small separations ($d_{\text{sep}}^{\text{proj}} < 1 h^{-1}\text{Mpc}$). At larger separations, however, the satellite distributions in 2D are slightly less bulging and lopsided than those in the mock catalog, with the discrepancy appearing to increase as $d_{\text{sep}}^{\text{proj}}$ increases. The relatively small differences found between

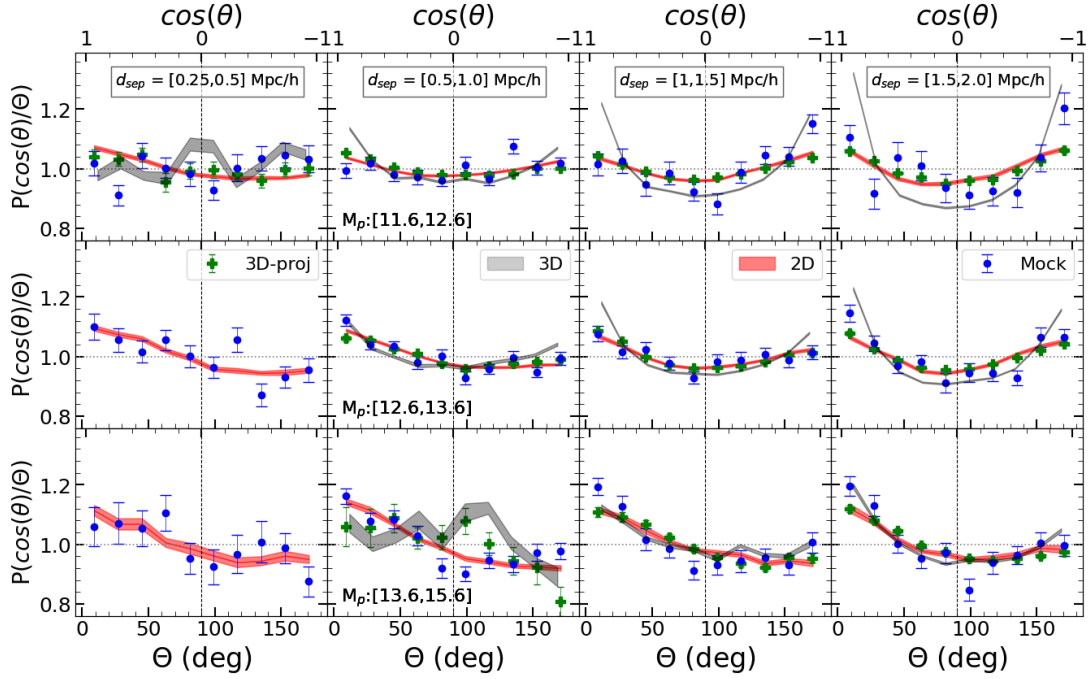


Figure 7. Satellite distribution $P(\Theta)$ obtained in 2D and from the mock catalog are shown in red shaded regions and blue dots, for halo pairs of different separations and primary halo masses, as indicated. For comparison, the 3D measurement $P(\cos\theta)$ and the 2D measurement of the halo pairs selected in 3D are plotted as grey shaded region and green dots, respectively.

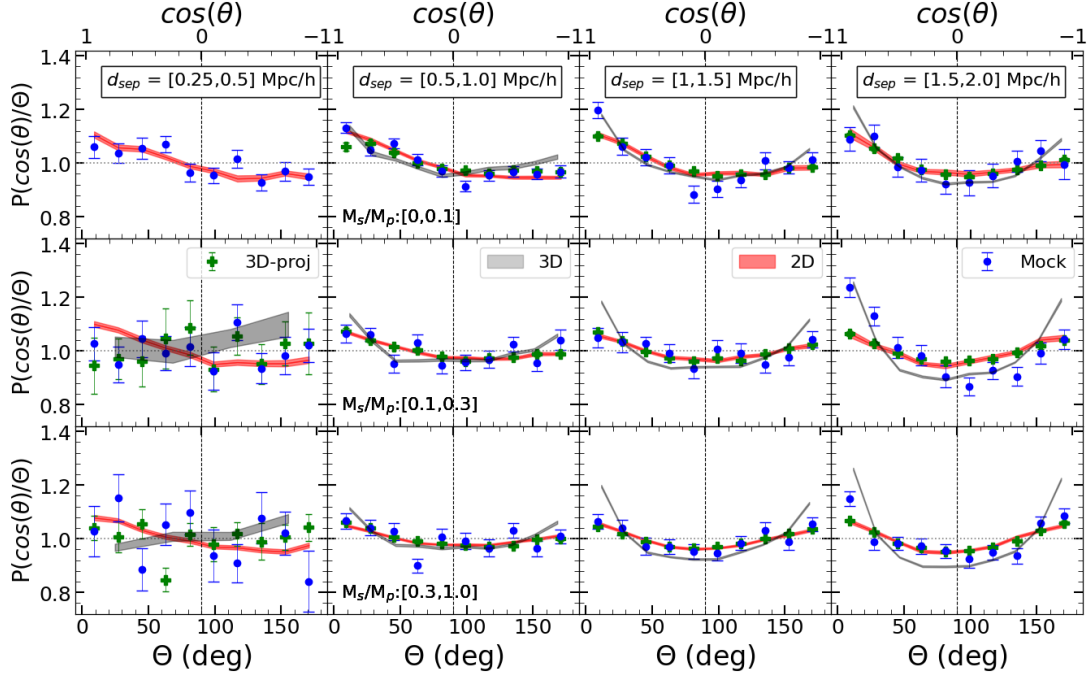


Figure 8. Same as the previous figure, but panels from top to bottom are for halo pairs of different secondary-to-primary halo mass ratios, as indicated.

the measurements from 2D and the mock catalog indicate that the 3D-to-2D projection is the dominant effect in a redshift survey like SDSS, and selection effects other than projection should not introduce significant biases,

provided they are properly accounted for in the statistical measurement, as we have done in both Paper I and this work.

For comparison, the 3D distribution measured by $P(\cos\theta)$ from the previous section is plotted as the grey shaded region in each panel. As expected, the 3D distribution is generally more strongly bulging than that measured in 2D and the mock catalog, particularly at large pair separations, low halo masses, and large halo mass ratios. For instance, as seen in the top-rightmost panel of Figure 7, the strongest bulging signal found in 3D for the most widely separated pairs of the lowest mass halos is dramatically suppressed by the projection effect, resulting in much weaker signals in the 2D plane and mock catalog. As a result, when transitioning from 3D to 2D and redshift space, the strong positive correlation of the bulging signal with pair separation is weakened, and the anti-correlation of the signal with halo mass is even reversed, leading to stronger bulging distributions around pairs of more massive halos. Furthermore, we notice that for pairs with the smallest separations ($d_{\text{sep}}^{\text{proj}} < 0.5 h^{-1}\text{Mpc}$), the tendency for a higher abundance of satellites on the outer sides of the halo pairs is also reversed by the projection effect.

One may wonder whether the differences observed between the 3D and 2D measurements arise not only from the projection effect but also from the different methods used to identify the halo pairs. To investigate this, we measure the distribution of the projected angle, i.e., $P(\Theta)$, for the halo pairs selected in 3D, and we present these measurements as green symbols in Figure 7 and Figure 8. As can be seen, these measurements agree very well with those from the 2D analysis (the red shaded regions), demonstrating that the different means of constructing halo pair samples contribute little to the differences observed between the 3D and 2D measurements.

3.2. Satellite distribution around overlapping halos

Now we further examine the influence of projection and observational selection effects on the overlap effect. Similar to the 3D analysis, we construct samples of overlapping halos with and without incorporating halo alignment, both in 2D and in the mock catalog. For the overlapping halos without alignment, two halos selected from the projection plane or the mock catalog are placed at the same projected separation and velocity difference as the corresponding halo pairs, and their halo masses are matched between the overlapping halos and the halos of the pair, using the same tolerance as adopted in the 3D analysis. For the overlapping halos that include alignment, we estimate the major axis of each halo in the projection plane from the projected inertia tensor, which is calculated from the second moment of mass derived from the projected particle distribution. The “aligned overlapping samples” in the projection plane

and the mock catalog are then constructed by rotating the major axes of the overlapping halos, along with their surrounding satellite distribution, so that the major axes of each pair of halos are aligned along their connection line.

For the overlapping halos without alignment, we find that the satellite distribution quantified by $P(\Theta)$ exhibits no significant differences among 3D, 2D, and the mock catalog for halo pairs with varying separations, halo masses, and mass ratios. For the aligned overlap samples, we observe that the bulging distribution found in 3D is significantly weakened in both 2D and the mock catalog due to the projection effect. In Figure 9 and Figure 10, the shaded regions in grey and green show the measurements of $P(\Theta)$ for the aligned overlapping halos in 3D and the mock catalogs. For clarity, we do not display the 2D measurements, as they are very close to those from the mock catalog. As can be seen, the weakening due to projection occurs by a factor that appears to be larger at smaller separations and for overlapping halo pairs with more massive halos and smaller mass ratios. As a result, the satellite distribution in the overlap samples from the mock catalog shows a rather weak dependence on halo pair properties, unlike the distribution in 3D, which exhibits strong variation in the bulging signal from panel to panel, as illustrated in the figures.

For comparison, the results for the actual halo pairs, as obtained earlier in 3D (red symbols) and from the mock catalog (blue symbols), are additionally shown in Figure 9 and Figure 10. In the mock catalog, the actual halo pairs and the overlapping halos demonstrate good agreement in satellite distribution across different halo pair properties. However, this agreement is coincidental and arises from the projection effect, which weakens the bulging signal in different ways for the actual pairs and the overlapping halos. Therefore, caution should be exercised when interpreting the observational distribution of satellites in halo pairs through the lens of the overlap effect.

4. DISCUSSION

4.1. Comparison with previous works

Previous studies of satellite distribution have focused on the MW-M31 system in the Local Group (McConnachie & Irwin 2006; Conn et al. 2013; Ibata et al. 2013), as well as its analogs in the nearby Universe (Libeskind et al. 2016) and in cosmological simulations (Pawlowski et al. 2017; Gong et al. 2019). The lopsided and bulging distribution of satellites observed in the Local Group is similarly observed for pairs of galaxies in the SDSS that broadly resemble the MW-M31 system (Libeskind et al. 2016). Additionally, cosmological

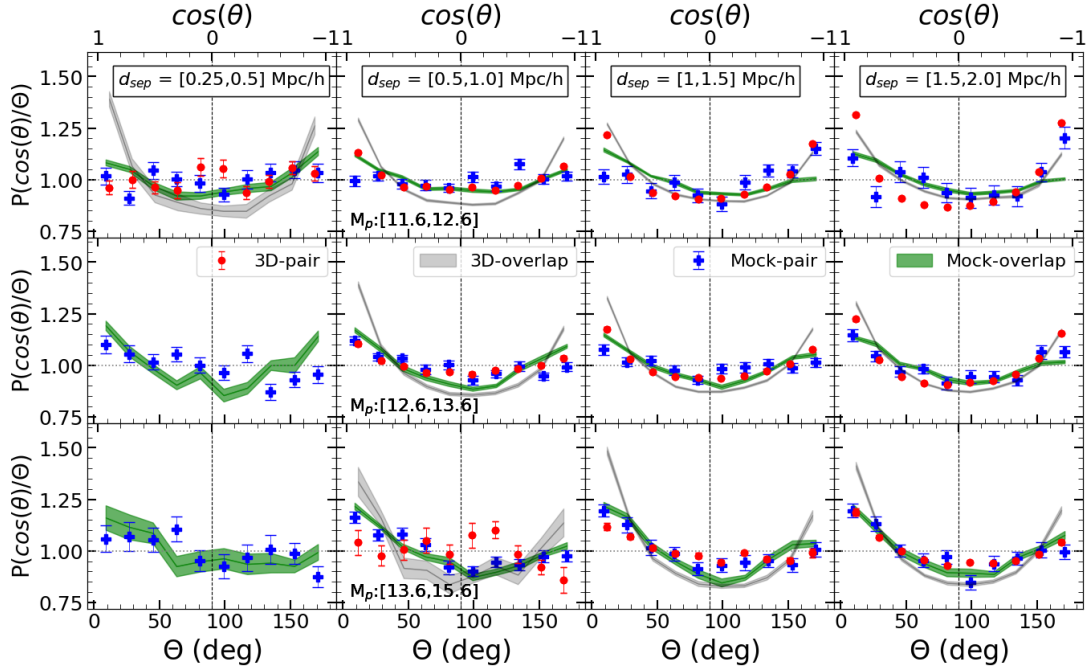


Figure 9. Measurements of satellite distribution are compared for actual halos in 3D (red), overlapping halos in 3D (grey), actual pairs in the mock catalog (blue) and overlapping halos in the mock catalog (green). Panels from left to right are for different pair separations, and those from top to bottom are for different primary halo masses, as indicated.

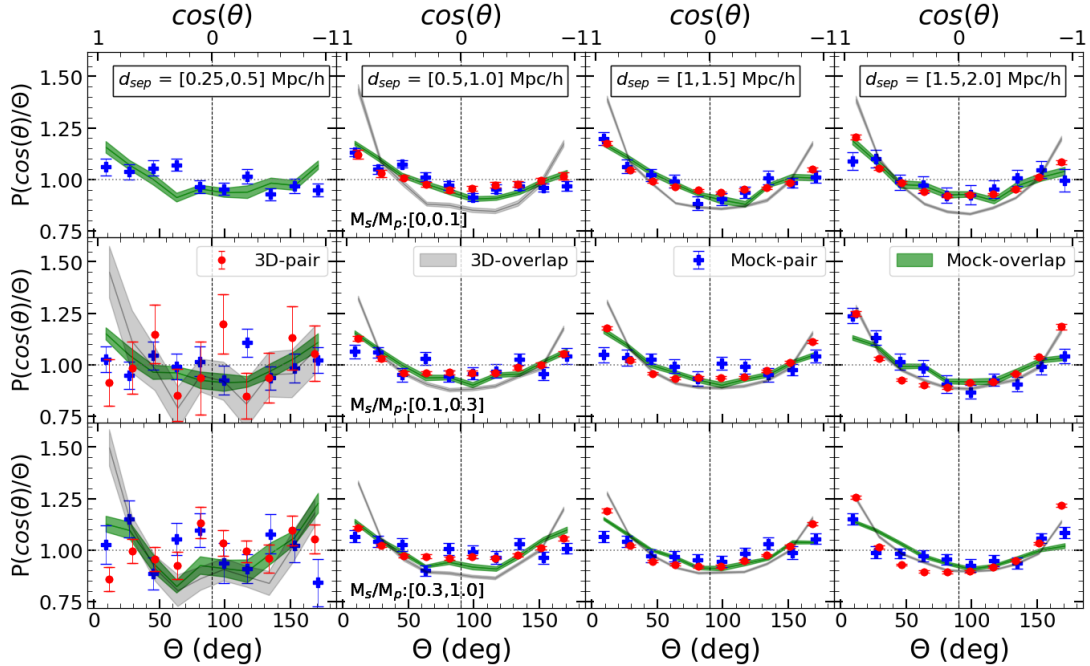


Figure 10. Same as the previous figure, but panels from top to bottom are for different secondary-to-primary halo mass ratios, as indicated.

simulations present similar satellite distributions around analogous halo pairs, demonstrating that the observational results are not purely caused by projection effects (Pawlowski et al. 2017; Gong et al. 2019). Furthermore,

by placing isolated halos at the same pair separations as the actual halo pairs, these studies have shown that the lopsidedness and bulging of satellites in the Local Group

and analogous systems cannot be simply attributed to the overlap effect.

Generally, our work yields results that are broadly consistent with those of previous studies for cases analogous to the MW-M31 system, specifically for the subsample of halo pairs with halo mass $11.6 \leq \log_{10}(M_p/M_\odot) \leq 12.0$ and pair separation $1.0 \leq d_{\text{sep}}/(h^{-1}\text{Mpc}) \leq 1.5$. The trends of bulging and lopsidedness signals with primary halo mass, halo mass ratio, pair separation, and satellite-to-host distance, as identified in our work, are consistent with those reported by Gong et al. (2019). In addition, we have performed the same test on the overlap effect as conducted in previous studies, and we also find that the satellite distribution around actual halo pairs cannot be explained by the overlap effect if the alignment of halo orientation is not taken into account, as was the case in previous investigations.

In this work, we have attempted to extend previous studies in several key aspects. Firstly, we consider more general cases of halo pairs beyond the Local Group by examining halo pairs with wider ranges of halo mass and pair separation. We find that the lopsided and bulging distributions are not limited to the MW-M31 analogs but are observed for halo pairs across broad ranges of halo mass and pair separation. Secondly, for the first time, we take into account the spatial alignment of halos when testing the overlap effect. We find that although the lopsidedness remains similar, the inclusion of halo alignment produces significant signals of bulging, thereby naturally reproducing the satellite distribution for halo pairs with varying properties. Additionally, we conduct comparisons between analyses conducted in 3D and 2D, as well as in the mock catalog, thus providing a comprehensive examination of the effect of projection and selection effects in observational samples.

4.2. *Implications for the origin of bulging and lopsidedness*

Our comparison between the 3D and 2D analyses demonstrates that, although the projection effect weakens the bulging distribution by a factor that depends on pair separation and halo mass, the bulging and lopsided distributions of satellites are fundamentally intrinsic behaviors of the halo pairs in a Λ CDM universe. More importantly, we find that the satellite distribution around halo pairs with varying properties can be reasonably well reproduced by the overlap effect, either with or without including the spatial alignment of halos. Specifically, the overlapping halos that do not consider halo alignment cannot produce any bulging signal, but they successfully replicate the satellite distribution for halo pairs

that are closely separated or involve massive halos. In contrast, the overlapping halos that are aligned with each other can produce significant bulging distributions that match the satellite distribution around halo pairs with relatively large separations and low halo masses.

As noted at the end of section 2, these results imply that the lopsidedness and bulging of the satellite distribution may arise from two distinct origins: the alignment of halo orientation with large-scale filaments is responsible for the bulging, while the overlap effect without alignment accounts for the lopsidedness. It is likely that the lopsidedness produced by the overlap effect is a ubiquitous phenomenon applicable to all halo pairs, exhibiting weak dependence on pair properties. In contrast, the bulging distribution generated by halo alignment is more dependent on the specific characteristics of the pairs. As a combined result of these two effects, the overall satellite distribution thus demonstrates varying strengths of lopsidedness and bulging across halo pairs with different properties.

The excess of matter between dark matter halo pairs has been well established in both simulations and observations, and this excess has indeed been utilized as a common method to identify filaments (Colberg et al. 2005; Clampitt et al. 2016; Epps & Hudson 2017; Xia et al. 2020; Kondo et al. 2020; Yang et al. 2022). Additionally, previous studies have found that galaxy pairs (Tempel & Tamm 2015; Mesa et al. 2018; Sarkar & Pandey 2024) and galaxy multiplets composed of small groups of 2-4 member galaxies (Rong et al. 2024; Laman et al. 2024) tend to align with their host filaments, with stronger alignment observed for more widely separated halo pairs (e.g. Tempel & Tamm 2015). Moreover, the thickness of filaments is found to be approximately 1-2 Mpc in the local universe (e.g. Aragón-Calvo et al. 2010; Bond et al. 2010; Cautun et al. 2014; Wang et al. 2024), which is consistent with our finding that the bulging signal dominates over the lopsidedness for wide pairs with $d_{\text{sep}} \gtrsim 1 h^{-1}\text{Mpc}$. All of these results align well with the idea that the bulging distribution has an alignment origin, as described above. This picture is also consistent with our finding that the bulging distribution is primarily contributed by subhalos that are relatively distant from their host halos, considering that the satellites in the outskirts of halos are more recently accreted and thus more capable of keeping their anisotropic distribution inherited from the filaments (Li et al. 2013; Gong et al. 2019; Liu et al. 2024).

Furthermore, although the alignment of isolated halos has previously been found to be positively correlated with halo mass (e.g. Faltenbacher et al. 2008), we find that the bulging of satellites becomes more pro-

nounced in halo pairs of lower masses at fixed pair separation. This implies that pairs of halos with relatively low masses are better tracers of the large-scale filamentary structures compared to those involving massive halos, which are preferentially located in high-density knots of the cosmic web that connect multiple filaments (e.g. Aragón-Calvo et al. 2010; Codis et al. 2018; Gouin et al. 2021).

4.3. Projection and selection effect

We have examined the effect of projection and observational sample selection on the satellite distribution in halo pairs by comparing the results obtained in 3D, 2D, and the mock catalog. The consistency between the 2D analysis and the mock catalog demonstrates that selection effects other than projection should not introduce significant biases, provided that the measurements are statistically corrected for those effects, as is done in both Paper I and this work. The 3D-to-2D projection significantly suppresses the bulging signals by a factor that depends on halo pair properties. Specifically, the suppression is particularly strong for widely separated pairs of low-mass halos. As a result, the anti-correlation of bulging with halo mass found in 3D turns into a positive correlation in the observational sample.

In addition, the 3D-to-2D projection affects the satellite distribution around actual halo pairs and that around overlapping halos in different ways. For instance, as can be seen from Figure 9, although the overlap sample and the actual pair sample agree well with each other when analyzed in 3D, their 2D measurements obtained with the mock catalog present significant discrepancies, particularly for widely-separated pairs of low-mass halos. This echoes the similar discrepancies found between halo pairs and overlapping halos from the SDSS galaxy sample; see Fig. 11 and discussion at the end of Section 4 in Paper I.

Therefore, caution should be exercised when interpreting the observational measurements of satellite distribution. The impact of projection cannot be easily corrected during statistical measurements, and a correct understanding can be achieved only by carrying out careful comparisons between model and data with the assistance of mock catalogs.

5. SUMMARY

In this work, we investigate the distribution of subhalos (satellites) in the vicinity of dark matter halo pairs within cosmological simulations. We utilize the Illustris-TNG300 dark matter-only simulation, from which we select a sample of halo pairs covering a wide range of primary halo mass, secondary-to-primary halo mass ratio,

and pair separation. We first perform three-dimensional (3D) measurements of the satellite distribution around the halo pairs, examining the dependence on pair separation, halo mass, mass ratio, and satellite-to-host distance. Next, we analyze the overlap effect by constructing samples of overlapping halos. In particular, we include the spatial alignment of halos in the overlap effect by aligning the major axes of the overlapping halos. Finally, we investigate the impact of projection and observational selection effects by conducting the same analysis of satellite distribution in two dimensions (2D) and in a mock catalog constructed from the same simulation, which replicates the selection effects of the SDSS galaxy sample as used in our Paper I (Guo, Ma & Li).

Our main findings can be summarized as follows.

1. The satellites around halo pairs with separations $d_{\text{sep}} > 0.5 h^{-1}\text{Mpc}$ present a non-uniform distribution in 3D. This distribution is a combined result of two distinct features: the “bulging” distribution, characterized by an overabundance along the connection line of the paired halos, and the “lopsided” distribution, which shows an overabundance in the region between the paired halos relative to the regions on the outer sides.
2. The bulging signal is stronger for halo pairs that are more widely separated and involve less massive halos, but it exhibits a rather weak dependence on the secondary-to-primary halo mass ratio. This signal is primarily contributed by subhalos that are relatively distant from their host halos.
3. Compared to the bulging, the lopsidedness shows weaker dependence on pair properties. Nevertheless, the lopsidedness strengthens as the primary halo mass increases, but it only weakly depend on pair separation. This signal also exhibits a weak dependence on the halo mass ratio and is primarily attributed to more distant subhalos.
4. The subhalos around close pairs with $d_{\text{sep}} < 0.5 h^{-1}\text{Mpc}$ appear to exhibit relatively uniform distributions, or even slightly higher abundances on the outer sides, though with large uncertainties.
5. The satellite distribution around halo pairs with varying properties can be reasonably reproduced by the overlap effect, provided that the spatial alignment of halos is properly taken into account. Specifically, overlapping halos without alignment can replicate the satellite distribution for halo pairs that are closely separated or involve massive halos, while overlapping halos that are aligned

with each other can produce strong bulging distributions that match the satellite distribution around halo pairs with large separations and low-mass halos.

6. Selection effects other than projection in real galaxy samples introduce negligible biases in the measurements of satellite distribution, but 3D-to-2D projection significantly suppresses the bulging signal, with particularly strong effect at large pair separations, low halo masses, and large halo mass ratios. This projection effect cannot be easily corrected, and a correct understanding can be

achieved only by carrying out careful comparisons between model and data with the help of mock catalog.

ACKNOWLEDGMENTS

. This work is supported by the National Key R&D Program of China (grant NO. 2022YFA1602902), the National Natural Science Foundation of China (grant Nos. 12433003, 11821303, 11973030), and China Manned Space Program through its Space Application System.

REFERENCES

- Allgood, B., Flores, R. A., Primack, J. R., et al. 2006, *MNRAS*, 367, 1781, doi: [10.1111/j.1365-2966.2006.10094.x](https://doi.org/10.1111/j.1365-2966.2006.10094.x)
- Aragón-Calvo, M. A., van de Weygaert, R., & Jones, B. J. T. 2010, *MNRAS*, 408, 2163, doi: [10.1111/j.1365-2966.2010.17263.x](https://doi.org/10.1111/j.1365-2966.2010.17263.x)
- Aubert, D., Pichon, C., & Colombi, S. 2004, *MNRAS*, 352, 376, doi: [10.1111/j.1365-2966.2004.07883.x](https://doi.org/10.1111/j.1365-2966.2004.07883.x)
- Bond, J. R., & Myers, S. T. 1996, *ApJS*, 103, 1, doi: [10.1086/192267](https://doi.org/10.1086/192267)
- Bond, N. A., Strauss, M. A., & Cen, R. 2010, *MNRAS*, 409, 156, doi: [10.1111/j.1365-2966.2010.17307.x](https://doi.org/10.1111/j.1365-2966.2010.17307.x)
- Brainerd, T. G., & Samuels, A. 2020, *ApJL*, 898, L15, doi: [10.3847/2041-8213/aba194](https://doi.org/10.3847/2041-8213/aba194)
- Cautun, M., van de Weygaert, R., Jones, B. J. T., & Frenk, C. S. 2014, *MNRAS*, 441, 2923, doi: [10.1093/mnras/stu768](https://doi.org/10.1093/mnras/stu768)
- Clampitt, J., Miyatake, H., Jain, B., & Takada, M. 2016, *MNRAS*, 457, 2391, doi: [10.1093/mnras/stw142](https://doi.org/10.1093/mnras/stw142)
- Codis, S., Pogosyan, D., & Pichon, C. 2018, *MNRAS*, 479, 973, doi: [10.1093/mnras/sty1643](https://doi.org/10.1093/mnras/sty1643)
- Colberg, J. M., Krughoff, K. S., & Connolly, A. J. 2005, *MNRAS*, 359, 272, doi: [10.1111/j.1365-2966.2005.08897.x](https://doi.org/10.1111/j.1365-2966.2005.08897.x)
- Conn, A. R., Lewis, G. F., Ibata, R. A., et al. 2013, *ApJ*, 766, 120, doi: [10.1088/0004-637X/766/2/120](https://doi.org/10.1088/0004-637X/766/2/120)
- Davis, M., Efstathiou, G., Frenk, C. S., & White, S. D. M. 1985, *ApJ*, 292, 371, doi: [10.1086/163168](https://doi.org/10.1086/163168)
- Doroshkevich, A. G. 1970, *Astrofizika*, 6, 581
- Epps, S. D., & Hudson, M. J. 2017, *MNRAS*, 468, 2605, doi: [10.1093/mnras/stx517](https://doi.org/10.1093/mnras/stx517)
- Faltenbacher, A., Jing, Y. P., Li, C., et al. 2008, *ApJ*, 675, 146, doi: [10.1086/525243](https://doi.org/10.1086/525243)
- Faltenbacher, A., Li, C., White, S. D. M., et al. 2009, *Research in Astronomy and Astrophysics*, 9, 41, doi: [10.1088/1674-4527/9/1/004](https://doi.org/10.1088/1674-4527/9/1/004)
- Forero-Romero, J. E., Contreras, S., & Padilla, N. 2014, *MNRAS*, 443, 1090, doi: [10.1093/mnras/stu1150](https://doi.org/10.1093/mnras/stu1150)
- Ganeshiah Veena, P., Cautun, M., van de Weygaert, R., et al. 2018, *MNRAS*, 481, 414, doi: [10.1093/mnras/sty2270](https://doi.org/10.1093/mnras/sty2270)
- Gong, C. C., Libeskind, N. I., Tempel, E., et al. 2019, *MNRAS*, 488, 3100, doi: [10.1093/mnras/stz1917](https://doi.org/10.1093/mnras/stz1917)
- Gouin, C., Bonnaire, T., & Aghanim, N. 2021, *A&A*, 651, A56, doi: [10.1051/0004-6361/202140327](https://doi.org/10.1051/0004-6361/202140327)
- Gu, Q., Guo, Q., Zhang, T., et al. 2022, *MNRAS*, 514, 390, doi: [10.1093/mnras/stac1292](https://doi.org/10.1093/mnras/stac1292)
- Heesters, N., Jerjen, H., Müller, O., Pawlowski, M. S., & Kanehisa, K. J. 2024, arXiv e-prints, arXiv:2406.11684, doi: [10.48550/arXiv.2406.11684](https://doi.org/10.48550/arXiv.2406.11684)
- Ibata, R. A., Lewis, G. F., Conn, A. R., et al. 2013, *Nature*, 493, 62, doi: [10.1038/nature11717](https://doi.org/10.1038/nature11717)
- Kang, X., & Wang, P. 2015, *ApJ*, 813, 6, doi: [10.1088/0004-637X/813/1/6](https://doi.org/10.1088/0004-637X/813/1/6)
- Knebe, A., Gill, S. P. D., Gibson, B. K., et al. 2004, *ApJ*, 603, 7, doi: [10.1086/381306](https://doi.org/10.1086/381306)
- Kondo, H., Miyatake, H., Shirasaki, M., Sugiyama, N., & Nishizawa, A. J. 2020, *MNRAS*, 495, 3695, doi: [10.1093/mnras/staa1390](https://doi.org/10.1093/mnras/staa1390)
- Lamman, C., Eisenstein, D., Forero-Romero, J. E., et al. 2024, arXiv e-prints, arXiv:2408.11056, doi: [10.48550/arXiv.2408.11056](https://doi.org/10.48550/arXiv.2408.11056)
- Li, Z., Wang, Y., Yang, X., et al. 2013, *ApJ*, 768, 20, doi: [10.1088/0004-637X/768/1/20](https://doi.org/10.1088/0004-637X/768/1/20)
- Libeskind, N. I., Frenk, C. S., Cole, S., et al. 2005, *MNRAS*, 363, 146, doi: [10.1111/j.1365-2966.2005.09425.x](https://doi.org/10.1111/j.1365-2966.2005.09425.x)
- Libeskind, N. I., Guo, Q., Tempel, E., & Ibata, R. 2016, *ApJ*, 830, 121, doi: [10.3847/0004-637X/830/2/121](https://doi.org/10.3847/0004-637X/830/2/121)
- Libeskind, N. I., Hoffman, Y., Knebe, A., et al. 2012, *MNRAS*, 421, L137, doi: [10.1111/j.1745-3933.2012.01222.x](https://doi.org/10.1111/j.1745-3933.2012.01222.x)

- Libeskind, N. I., Hoffman, Y., Tully, R. B., et al. 2015, MNRAS, 452, 1052, doi: [10.1093/mnras/stv1302](https://doi.org/10.1093/mnras/stv1302)
- Libeskind, N. I., Knebe, A., Hoffman, Y., & Gottlöber, S. 2014, MNRAS, 443, 1274, doi: [10.1093/mnras/stu1216](https://doi.org/10.1093/mnras/stu1216)
- Liu, Y., Wang, P., Guo, H., et al. 2024, MNRAS, 529, 1405, doi: [10.1093/mnras/stae625](https://doi.org/10.1093/mnras/stae625)
- Marinacci, F., Vogelsberger, M., Pakmor, R., et al. 2018, MNRAS, 480, 5113, doi: [10.1093/mnras/sty2206](https://doi.org/10.1093/mnras/sty2206)
- McConnachie, A. W., & Irwin, M. J. 2006, MNRAS, 365, 902, doi: [10.1111/j.1365-2966.2005.09771.x](https://doi.org/10.1111/j.1365-2966.2005.09771.x)
- Mesa, V., Duplancic, F., Alonso, S., et al. 2018, A&A, 619, A24, doi: [10.1051/0004-6361/201832910](https://doi.org/10.1051/0004-6361/201832910)
- Naiman, J. P., Pillepich, A., Springel, V., et al. 2018, MNRAS, 477, 1206, doi: [10.1093/mnras/sty618](https://doi.org/10.1093/mnras/sty618)
- Nelson, D., Pillepich, A., Springel, V., et al. 2018, MNRAS, 475, 624, doi: [10.1093/mnras/stx3040](https://doi.org/10.1093/mnras/stx3040)
- Okumura, T., Jing, Y. P., & Li, C. 2009, ApJ, 694, 214, doi: [10.1088/0004-637X/694/1/214](https://doi.org/10.1088/0004-637X/694/1/214)
- Pawlowski, M. S., Ibata, R. A., & Bullock, J. S. 2017, ApJ, 850, 132, doi: [10.3847/1538-4357/aa9435](https://doi.org/10.3847/1538-4357/aa9435)
- Paz, D. J., Sgró, M. A., Merchán, M., & Padilla, N. 2011, MNRAS, 414, 2029, doi: [10.1111/j.1365-2966.2011.18518.x](https://doi.org/10.1111/j.1365-2966.2011.18518.x)
- Peebles, P. J. E. 1969, ApJ, 155, 393, doi: [10.1086/149876](https://doi.org/10.1086/149876)
- Pillepich, A., Nelson, D., Hernquist, L., et al. 2018, MNRAS, 475, 648, doi: [10.1093/mnras/stx3112](https://doi.org/10.1093/mnras/stx3112)
- Rong, Y., Shen, J., & Hua, Z. 2024, MNRAS, 531, L9, doi: [10.1093/mnrasl/slae021](https://doi.org/10.1093/mnrasl/slae021)
- Samuels, A., & Brainerd, T. G. 2023, ApJ, 947, 56, doi: [10.3847/1538-4357/acc069](https://doi.org/10.3847/1538-4357/acc069)
- Sarkar, S., & Pandey, B. 2024, arXiv e-prints, arXiv:2407.16675, doi: [10.48550/arXiv.2407.16675](https://doi.org/10.48550/arXiv.2407.16675)
- Schneider, M. D., Frenk, C. S., & Cole, S. 2012, JCAP, 2012, 030, doi: [10.1088/1475-7516/2012/05/030](https://doi.org/10.1088/1475-7516/2012/05/030)
- Shao, S., Cautun, M., Frenk, C. S., et al. 2018, MNRAS, 476, 1796, doi: [10.1093/mnras/sty343](https://doi.org/10.1093/mnras/sty343)
- Springel, V., White, S. D. M., Tormen, G., & Kauffmann, G. 2001, MNRAS, 328, 726, doi: [10.1046/j.136F5-8711.2001.04912.x](https://doi.org/10.1046/j.136F5-8711.2001.04912.x)
- Springel, V., Pakmor, R., Pillepich, A., et al. 2018, MNRAS, 475, 676, doi: [10.1093/mnras/stx3304](https://doi.org/10.1093/mnras/stx3304)
- Tempel, E., Guo, Q., Kipper, R., & Libeskind, N. I. 2015, MNRAS, 450, 2727, doi: [10.1093/mnras/stv919](https://doi.org/10.1093/mnras/stv919)
- Tempel, E., & Tamm, A. 2015, A&A, 576, L5, doi: [10.1051/0004-6361/201525827](https://doi.org/10.1051/0004-6361/201525827)
- Wang, K., Avestruz, C., Guo, H., Wang, W., & Wang, P. 2024, MNRAS, 532, 4616, doi: [10.1093/mnras/stae1805](https://doi.org/10.1093/mnras/stae1805)
- Wang, P., Libeskind, N. I., Pawlowski, M. S., et al. 2021, ApJ, 914, 78, doi: [10.3847/1538-4357/abfc4f](https://doi.org/10.3847/1538-4357/abfc4f)
- Wang, Y., Yang, X., Mo, H. J., et al. 2008, MNRAS, 385, 1511, doi: [10.1111/j.1365-2966.2008.12927.x](https://doi.org/10.1111/j.1365-2966.2008.12927.x)
- Wang, Y. O., Lin, W. P., Kang, X., et al. 2014, ApJ, 786, 8, doi: [10.1088/0004-637X/786/1/8](https://doi.org/10.1088/0004-637X/786/1/8)
- White, S. D. M. 1984, ApJ, 286, 38, doi: [10.1086/162573](https://doi.org/10.1086/162573)
- Xia, Q., Robertson, N., Heymans, C., et al. 2020, A&A, 633, A89, doi: [10.1051/0004-6361/201936678](https://doi.org/10.1051/0004-6361/201936678)
- Yang, T., Hudson, M. J., & Afshordi, N. 2022, MNRAS, 516, 6041, doi: [10.1093/mnras/stac2564](https://doi.org/10.1093/mnras/stac2564)
- York, D. G., Adelman, J., Anderson, John E., J., et al. 2000, AJ, 120, 1579, doi: [10.1086/301513](https://doi.org/10.1086/301513)
- Zentner, A. R., Kravtsov, A. V., Gnedin, O. Y., & Klypin, A. A. 2005, ApJ, 629, 219, doi: [10.1086/431355](https://doi.org/10.1086/431355)
- Zhang, Y., Yang, X., Faltenbacher, A., et al. 2009, ApJ, 706, 747, doi: [10.1088/0004-637X/706/1/747](https://doi.org/10.1088/0004-637X/706/1/747)